Advanced Control to Damp Power Oscillations with VSC-HVDC Links Inserted in Meshed AC grids

Yankai Xing, Elkhatib Kamal, Bogdan Marinescu, Florent Xavier

ORIGINAL ARTICLE

Journal Section

Advanced Control to Damp Power Oscillations with VSC-HVDC Links Inserted in Meshed AC grids

Yankai Xing[1]* | **Elkhatib Kamal**[1]* | **Bogdan Marinescu**[1]* | **Florent Xavier**[2]†

[1]Ecole Centrale de Nantes, LS2N-CNRS, 1 rue de la Noë, Nantes, France

[2]R&D Division, RTE, Paris La Défense, France

Correspondence
Bogdan Marinescu, 1 rue de la Noë, 44300 Nantes, France
Email: Bogdan.Marinescu@ec-nantes.fr

Funding information

In this paper, we consider the particular situation of a HVDC link inserted in a meshed AC grid which have inter-area modes at upper frequencies than the usual ones. In this case, the standard IEEE (lead-lag plus gain) controllers may not be efficient. As a matter of fact, in this grid situation, the control is challenged by unstable zeros and system uncertainties, systematically put into evidence. Two original robust strategies based on matching a reference model using LMI optimization approach are designed to provide coordinated active and reactive power modulation for the HVDC link. They are based on a reduced order control model of the HVDC and the neighboring AC zone which integrates the dynamics of interest. Besides increased damping and diminished impact of the unstable zeros, this new control achieves robustness against grid variations. Investigations with both linearized and nonlinear model of the system are carried out to settle and validate the approach. The efficiency and robustness of the proposed controllers are tested and compared with the ones of several standard controllers on a realistic benchmark of 19 generators interconnected by a meshed AC grid.

KEYWORDS

Abbreviations:

* Equally contributing authors.

Power system oscillations, HVDC, damping controller, inter-area modes, robustness.

1 | INTRODUCTION

Electromechanical oscillations are a major concern of today power grids. This is a problem of power system oscillatory stability, as shown, for example, in Europe in December 2016 when low damping oscillations related to the most spread inter-area mode (at 0.15Hz) have been experienced [1]. When provided with supplementary damping control, the HVDCs have a good damping effect, which can be used to solve the problem of low frequency oscillations between regions. Especially, VSC (Voltage Source Converters)-HVDC transmission systems have the advantage to control both active and reactive power. This provides the opportunity to maintain system stability through supplementary POD (Power Oscillations Damping) loops of control for both active and/or reactive power modulations [2].

The most analyzed and controlled in the past were the most spread inter-area modes of the interconnected system which are the ones in which are involved a large number of generators. They are at low frequencies, for example, around 0.2 Hz in Europe. Recent HVDC reinforcements in Europe (like France-Italy interconnection) are in the oscillation path of inter-area modes of higher frequencies, around 1Hz. There are also other dynamics of the grid in this frequency range (see [3] and [4]). These different dynamics should be taken into account more directly than in classic POD controllers (IEEE structures) and methodologies for gain computation (like, e.g., [5]).

Unstable zeros in the system can bring some delays in the outputs of the system [6]. The appearance of unstable zeros in a AC grid model which contains an HVDC link has been analyzed in the former research [7]. In addition, plant models are usually subject to modeling errors and uncertainties. In our case, these are due to variation of the grid operating point due to typical scenarios like, for example, generator and line trips, change of the amount of power transferred by the HVDC link, etc.

To ensure robustness of the controls in the grid context and situations mentioned above, the control model based only on sensitivities of the modes to be damped against the gain of the controller usually used in classic POD controller synthesis (e.g., [5] or [8]) is no longer sufficient. The most advanced control methods use a state-space representation of the plant (see, e.g., [9]). Current for small-size systems, such a representation is difficult to be provided in order to capture the inter-area modes of large interconnected grids. As a matter of fact, a detailed modeling of all generators (or dynamic devices) is needed in this case and standard model reduction (like based on balanced realization state truncation [9] or Schur balanced model reduction [10]) cannot be directly applied because of their weak rate of reduction with respect to performances (preservation of inter-area modes). In [11], an aggregation methodology was proposed as an alternative to focus on a given frequency interval which contain the frequencies of the targeted inter-area modes. This methodology has been used here to gather the modes to be damped and the other modes of grid which may be affected by the POD controller into a small-size *control model*.

H_∞ and H_2 control are important and traditional advanced robust control techniques. They belong to a frequency domain approach which allows the designer to settle a good trade-off between specifications of the control (performances) and sensitivity of the closed-loop with respect to model errors and disturbances (robustness) [12]. Robustness is quantified in norm-bounded uncertainty or polytopic uncertainty [13], [14]. The latter are integrated as constraints in optimization problems that provide the controller gains. The latter problems are solved by well established and numerically reliable Linear Matrix Inequality (LMI) methodologies [15], [16] . Advanced controls have already been used to damp power oscillations with HVDCs. The survey given in [17] put into evidence H_2 [18] and Model Predictive controls [19]. However, it is a well known fact in automatic control that these methods loose their efficiency in case of

unstable zeros close to origin [9]. This will be shown in this paper for the case of the HVDC. Moreover, the existence of the unstable zeros in the case of an HVDC inserted in meshed AC grid was very recently put into evidence [23]. Their location varies with the grid disturbances and nonlinearities. The new control problem with this combined specifications (modes damping, robustness and cancellation of unstable and uncertain zeros effect) is hard to solve and not tackled in the today's existing literature. For this, we propose here a new control framework which consists in a combination of aforementioned robust controls and *model matching of the closed-loop*.

Model-matching is a method to force the closed-loop to provide a desired structure and dynamics (see, e.g., [20]). More specifically, starting from desired performances of the closed-loop (the specifications of the control), a desired input-output (transfer matrix or state-space) model is deduced. The regulator is next synthesized to provide a closed-loop input-output behavior as close as possible to the one of the desired model. This is an optimization problem which can be solved in several ways, according to the type of chosen regulator (H_∞, H_2, ...). Two original H_∞-based model-matching controller schemes via static and dynamic output-feedback -Robust Static Output-error Feedback Controller (RSOFC) and Dynamic Decoupling Output-Feedback Controller (DDOFC)- are proposed here. They ensure the aforementioned *extended specifications*, more specifically:

- damp high-frequency inter-area modes
- overcome the effect of unstable zeros
- tolerate variations of the grid conditions (like load and topology variations, modification of the load flow, variation of the volume and direction of the transit through the DC line, tripping of lines and generators, ...)
- tolerate major grid faults (like severe short-circuits) which excite nonlinearities

For the synthesis of the controllers, Lyapunov-type sufficient conditions are translated in terms of LMIs. The latter are constructive in the sense that the RSOFC and DDOFC gains are found by solving these LMIs. Full nonlinear simulations in comparison with classic robust controllers are done for validation. For these comparison needs, strategies, like LQG controller and mixed sensitivity H_∞, are briefly recalled in the paper.

The rest of the paper is organized as follows: Section II formulates the power systems problem, main difficulties and modeling. Several robust control strategies are tuned in Section III. Model-matching LMI-based design is given in Section IV for *static* and *dynamic* output feedback. Section V is devoted to validations. In Section VI the approach is extended to the coordination of P/Q controllers. Concluding remarks are given in Section VII.

2 | POWER SYSTEM MODELING AND PROBLEMS FORMULATION

2.1 | System modeling and test system

2.1.1 | HVDC models

Figure 1 shows a typical embedded VSC- HVDC that consists of two main converter stations; one station operates as a controlled rectifier and the other operates as a controlled inverter station. The two converter stations use bidirectional three-phased (voltage-source) AC-DC power converters and are modeled as current or power injectors. To deal with a computational method for transient dynamic analysis which enables one to cover the low frequency ranges, two models (model I and model II) are used in this work. In *model I*, the Electromagnetic Transients (EMT) modeling and HVDC transient model of injections are considered based on [21]. *Model II* is a low-frequency one for transient dynamics. Therefore, phase angle θ of the voltage source and the magnitude U_{ac} can be controlled. P_1, P_2 and Q_1, Q_2

are respectively active and reactive powers exchanged with the power system.

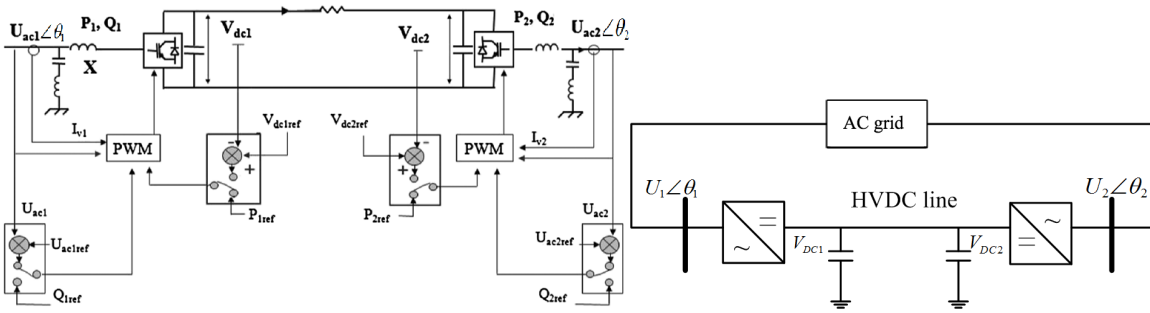

FIGURE 1 HVDC model and HVDC inserted in an AC grid.

2.1.2 | HVDC link embedded in a large-scale AC grid

The studied HVDC link embedded in a large-scale AC grid is given in Fig. 1. The situation becomes particular when the AC grid is highly meshed and inter-area modes are of higher frequencies as the ones in Table 1. To damp such modes, the proposed DDOFC is designed based on a well-chosen *control model*. As a consequence, the DDOFC does not disturb the other modes are near in frequency of the targeted inter-area modes and is more robust against the neglected dynamics at higher frequencies. Moreover, the damped modes and the other modes are considered in *control model*. The control model consists thus of HVDC dynamics and the aforementioned near frequency dynamics of the grid and is given by the transfer matrix $H(s)$ of Fig. 3 and 4. The benchmark proposed in this work sums-up these problems. It is composed of an HVDC line (HVDC model I) in a meshed AC grid with order 724 which consists of 19 generators (Fig. 2). Each generator is equipped with AVR and PSS controls. The *full linear model* is obtained by linearizing this model at a chosen operating point using Eurostag software [21].

From the Fig. 3 and 4, it can be seen that the modes to be damped have high residues in transfer function $H(s)$. The highest residues modes and most participating machines of the full linear model are given in Table 1 where the damping and frequency are presented for each mode. GE_911 and GE_917 are the most participating generators to mode 2 which are swinging one against the other. The magnitude of participation factors evaluate the contribution of each generator to the modes. 100% participation factor means that the corresponding generator is the most participating machine in the considered mode. From Table 1, it can be seen that the less damped (4.5%) inter-area mode is mode 2 which is at 0.88Hz. It should be noticed that the other listed inter-area modes are at near frequencies. They are highly damped (modes 6 to 10) or poorly damped (modes 1 to 5). Notice also that in this frequency band there are also *local modes* like mode 8 (which is not an inter-area mode because it is related to generators (GE_921, GE_922) which are in the same area). The pattern of oscillation of mode 2, the less damped one, corresponds to areas A and B indicated in Fig. 2.

2.2 | Control model

Two strategies are possible to design the *control model*. For the first one, a *reduced order model* of the HVDC and the neighboring AC zone with around 10 state variables is developed from a full model with order 724. The second method

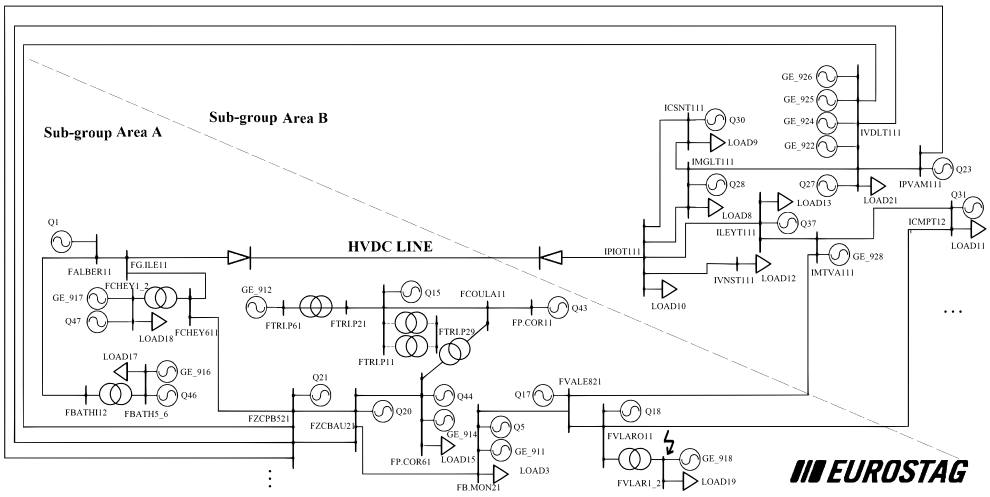

FIGURE 2 The benchmark model.

consists in *aggregation* around the modes of interest, that is, the curve fitting of Bode plot with information of modes of interest as given in [22]. This leads to a low order transfer matrix $H(s)$ control model even in case of large systems and was thus adopted here (numerical results are given in Appendix B).

The terminal difference of angles, $\Delta\theta = \theta_1 - \theta_2$, has the highest *residue* as control signal in our case and it is thus selected as input of the regulator: $y = \Delta\theta$ ([23]). It is measured by standard PLL techniques.

The output of the controller u is Q, the reactive power. It will be extended in Section 6 to a mixed P/Q modulation.

The POD is implemented as a supplementary higher (second) level control loop (see, e.g., [5], [25]) as shown in Fig. 3. The basic regulation loops called *first-level control* in the same figure are to control the HVDC converter to fulfill local objectives (like control the voltage, current and power transmission).

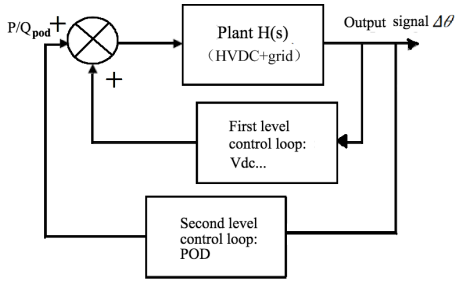

FIGURE 3 Control loops for the HVDC link.

2.3 | Classic POD and its limitations

The classic POD inherits the structure of PSS for generators as shown in Fig. 4. Its transfer function is

TABLE 1 The linearized model

No.	Mode	Damping ξ (%)	Freq. (Hz)	Mode shape (participation mag (%))		Residue	
				+	−	ABS MAG	Phase
1	-1.62+j8.19	19.5	1.30	GE_914 (100)	GE_913 (32.4)	0.0157	35.0
2	**-0.24+j5.53**	**4.5**	**0.88**	**GE_911 (100)**	**GE_917 (68.8)**	**0.0181**	**83.4**
3	-0.53+j5.29	10.1	0.84	GE_917 (100)	GE_918 (55.1)	0.0129	-56.2
4	-0.40+j4.79	8.3	0.76	GE_918 (44.3)	GE_912 (100)	0.0038	-33.3
5	-0.33+j3.29	10.1	0.52	GE_915 (100)	GE_918 (17.7)	0.0121	104.5
6	-18.83+j7.21	93.3	1.14	GE_921, GE_922 (100)	GE_923, GE_924 (74.1)	0.0034	14.5
7	-1.54+j6.55	22.9	1.04	GE_914 (100)	GE_911 (68.3)	0.0125	151.5
8	-19.32+j6.47	94.8	1.03	GE_921 (100)	GE_922 (37.6)	0.0117	118.9
9	-20.33+j4.86	97.2	0.77	GE_921, GE_922 (84.5)	GE_927 (100)	0.0026	-168.1
10	-18.72+j3.35	98.4	0.53	GE_913 (33.4)	GE_912 (100)	0.0072	136.1

$$H_{POD}(s) = K\left(\frac{T_w s}{1+T_w s}\right)\left(\frac{1+T_1 s}{1+T_2 s}\right)^n, \tag{1}$$

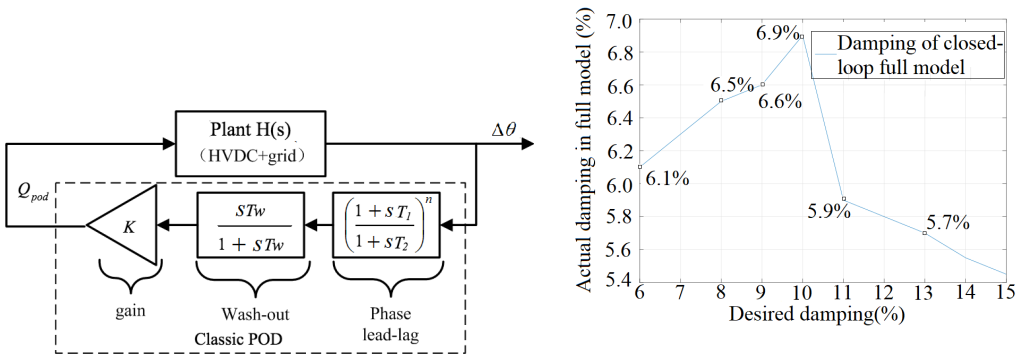

FIGURE 4 Structure of classic POD, desired and obtained dampings (classic POD).

where K is the gain, n is the number of phase lead-lag blocks. The washout filter is used to reject the steady-state component of the measures output [24]. The POD parameters K, T_1, and T_2 are calculated as the following [25]:

- *i)* T_1 and T_2 are calculated in order to shift the phase of the mode residue to 180°.
- *ii)* the desired damping is next obtained adjusting the gain K.

Values $K = 2.5614$; $T_1 = 0.4746$; $T_2 = 0.0688$; $T_w = 1$; $n = 2$ were obtained when targeting mode 2 of the considered benchmark. This strategy can be easily used for one mode. However, its multiband extension [26], cannot be fully exploited in our case because this method requires that the considered frequency bands are well separated to make

sure that the each band is not influencing the others. Nevertheless, the only information used from the grid is the residue of the targeted mode for damping. As a consequence, in principle, to obtain high desired damping one has to use high gains in the control loop. This contradicts robustness principles and may lead to closed-loops with limited or even opposite results. Table 2 and Fig 4 shows the relationship between the desired damping and the obtained damping in the closed-loop. Indeed, for desired damping superior to 6 %, the really obtained damping increases from around 6% to around 7% and after decreases.

TABLE 2 The relationship between desired damping and closed-loop obtained damping in the full linearized system (classic POD)

Desired damping (%)	6	7	8	9	10	11	12	13	14	15
Actual lowest damping (%) in full model closed-loop	6.1	6.3	6.5	6.6	6.9	5.9	5.8	5.7	5.5	5.4

This means that, for example, a desired damping of 10% cannot be reached with a classic POD. Tuning for this value results in $K = 2,56$, $T_1 = 0,47$, $T_2 = 0,06$, $T_w = 1$, $n = 2$ and the obtained closed-loop dampings are given in Table 3. The obtained damping for mode 2 is only 6%. From Table 3, it can be seen that the damping of mode 1 is improved despite the fact that this was not the target of the tuning. This situation is not always favourable. For example, damping of mode 4 is worse than without POD.

TABLE 3 Comparison of damping of modes

No.mode	Damping without POD (%)	Damping of modes with classic POD (%)
1	19.5	30.5
2	4.5	6.1
3	10.1	12.0
4	8.3	8.1
5	10.1	12.4

To overcome these difficulties, advanced controllers are proposed based on a state-space approach which is more performant (from the damping point of vue) and more robust against the usual changes of the grid mentioned in the Introduction.

2.4 | Problem of unstable zeros

In the control of non-minimum-phase systems (i.e., transfer functions with unstable zeros), it is necessary to suppress the negative tuning caused by the unstable zeros and reduce the adjustment time of the system. More specifically, in this case, poles of the closed-loop move toward zeros, and thus destabilization inevitably occurs. Hence, the closed-loop has limited gain margin when the open-loop transfer function has unstable zeros, which cause performances limitation [6]. Thus, it is necessary to identify the unstable zeros in the studied system and to propose a strategy to eliminate their negative effects. First, a benchmark was proposed in [23] to take into account a large number of structures and

oscillation paths in order to establish a link between the parameters of the benchmark and existence of open-loop unstable zeros. Next, in [7], a Modified Zero Phase Error Compensator (MZPEC) was proposed to cancel the negative effect of unstable zeros. The introduced MZPEC is free of the controller type applied and it can be designed with the advanced POD controllers (i.e., Linear Quadratic Gaussian (LQG) or H_∞) to cancel unstable zeros to improve the dynamic responses. However, it was shown that the position of the unstable zeros change during large disturbances like the short-circuits. The MZPEC compensator has difficulties to face such disturbances as well as evolution of the model like, e.g., cases of different operation points. Thus, more robust controllers are proposed here.

3 | LIMITATIONS OF DIRECT APPLICATION OF ROBUST CONTROL

In order to position the new proposed controllers against existing solutions, the LQG and mixed sensitivity H_∞ controllers are recalled in this section and used for comparison purposes. They are developed in our former work in details in [27], [22].

All of them use a state-representation of $H(s)$ in Fig. 3 of the form

$$\begin{aligned} \dot{x} &= Ax + Bu \\ y &= Cx, \end{aligned} \tag{2}$$

where $x \in \Re^{n\times 1}$, $y \in \Re^{g\times 1}$ and $u \in \Re^{m\times 1}$ are, respectively, the state, output and the control input. $C \in \Re^{g\times 1}$, $A \in \Re^{n\times n}$, $B \in \Re^{m\times n}$.

3.1 | Robust control

3.1.1 | LQG

The LQG approach (e.g., [9], [28]) proposes a control which minimizes

$$J_{LQG} = E\left\{\lim_{T\to\infty}\frac{1}{T}\int_0^T [x^T Qx + u^T Ru]dt\right\}, \tag{3}$$

where Q and R are appropriately chosen constant weighting matrices design parameters such that $Q = Q^T > 0$ and $R = R^T > 0$.

The LQG POD scheme of our case is shown in Fig. 5. The same kind of wash-out filter used in classic POD is added and taken into account in the synthesis of the gains of the LQG controller. More specifically, this filter is incorporated into the plant model H'(s) from which it is computed the state-space (2) used for the gains synthesis.

The resulting transfer function of the regulator is:

$$Q_{pod} = -K_r\hat{x} = -K_r(sI - A + LC)^{-1}\begin{pmatrix} B & L \end{pmatrix}\begin{pmatrix} u \\ \Delta\theta_w \end{pmatrix} \tag{4}$$

where K_r is the *LQ control gain* and L is the *estimation gain of the Kalman filter*. Each of them are computed by Matlab function lqr which solves a specific Riccati equation.

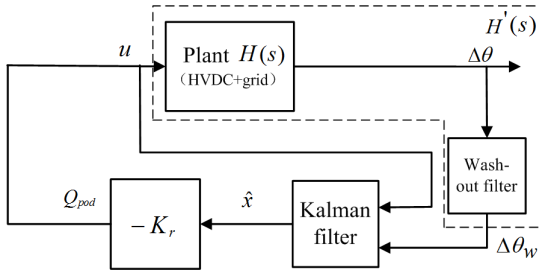

FIGURE 5 The implemented control structure of LQG method.

3.1.2 | Mixed sensitivity H_∞ with LMI controller

The structure of the mixed sensitivity H_∞ controller is given in Fig. 6. The standard H_∞ optimal control problem is to find all stabilizing controllers $K(s)$ which minimize the input-output transfer of the *augmented plant* $H'(s)$.

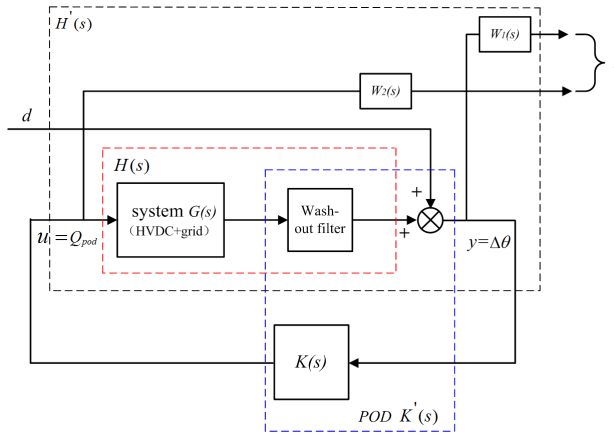

FIGURE 6 Controller structure of mixed sensitivity H_∞ with LMI.

More specifically, the objective is to stabilize the closed-loop and minimize

$$\left\| \begin{bmatrix} W_1(s)S(s) \\ W_2(s)KS(s) \end{bmatrix} \right\|_\infty < \gamma, \tag{5}$$

where d is the input disturbance, z is the controlled output, γ is minimum value of (5) over all stabilizing controllers $K(s)$.

The state-space parameters of controller $K(s)$ can be found via solving three LMIs. The target damping can be designed by transferring the desired damping information to one of the LMIs (see details in [22]).

3.2 | Performance and robustness analysis

Control of power systems is a complex problem because of the multivariable aspect and parameter uncertainties. The matter may come with the change of environment (load or generation level evolution, line trips, etc.), ageing of components, measurement errors, etc.. Parameter uncertainties make the values of the parameters deviate from the nominal values and may degrade the performance or even cause instability of the closed-loop system. In general, these uncertainties are difficult to measure. From the control point of view, such variation results in deviation of some elements of the A, B, C matrices of the linearized state model (2) from their nominal values. They should be counteracted by increased robustness properties of the controllers.

It is well known that there is a trade-off between the performances and robustness of a controller. Therefore, in order to achieve the required damping and satisfy robustness, this trade-off should be investigated. Due to the advantage of direct desired damping specification of mixed sensitivity H_∞ strategy, it is discussed as an example in this section the relationship between performances and robustness. Table 4 presents the dampings estimated with the control model against the ones really obtained with the mixed sensitivity H_∞ full closed-loop model. All the modes of damping higher than 6% (value which corresponds to the lowest damping obtained with classic POD) are presented. In this table and Fig. 7, it can be seen that the lowest damping of the modes of the control model closed-loop increases with the desired damping, but the damping of closed-loop for full model is limited to a maximum value (11.86%) due to the modeling error. Thus, $\beta = 167°$ (β is the angle of conics in left complex plane directly correlated with damping ratio $\xi = \cos\frac{\beta}{2}$ (see Fig. 8)). One can thus first conclude that, in general, robustness should be improved by proposing a better control methodology. Next, once the control methodology adopted, the synthesis of the parameters of the regulator should be done with a reasonable trade-off between performances-damping in our case-and robustness. This means that one should not try to maximize the damping in order to have a good level of robustness. This means that damping target should be fixed to the minimum acceptable level from the physical and technological point of view. The robustness of the resulting closed-loop will be thus maximal in order to fulfill the other control objectives specified in Section 2.

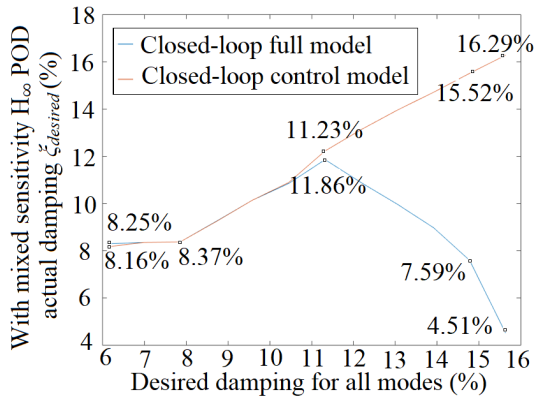

FIGURE 7 Difference between desired (control model) and obtained (full model) damping of the closed-loop.

TABLE 4 The relationship between desired damping for all modes and obtained mixed sensitivity H_∞ closed-loop lowest damping among all modes

Desired damping(%) (Angle β (deg) in the complex plane)	Obtained lowest damping (%) in closed-loop control model	Obtained lowest damping (%) in closed-loop full model
6.1 (173)	8.16	8.25
6.9 (172)	8.35	8.35
7.8 (171)	8.37	8.37
8.72 (170)	9.24	9.25
9.5 (169)	10.14	10.14
10.4 (168)	10.89	10.85
11.3 (167)	**12.23**	**11.86**
12.1 (166)	13.14	10.88
13 (165)	13.96	9.97
13.92 (164)	14.72	8.97
14.78 (163)	15.52	7.59
15.64 (162)	16.29	4.51

4 | MODEL-MATCHING ROBUST H_∞ OUTPUT-FEEDBACK CONTROL

It is known that the model-matching control is a method which uses feedback control to force the closed-loop model to follow a pre-specified, i.e., desired *reference model*. To satisfy requirements formulated aforementioned, two model-matching control design methods for HVDC systems based on the LMIs technique are now proposed: ROSFC and DDOFC. Both methods use a reference model which is built from the desired specifications (damping, poles, zeros). A feedback is next synthesized to force the plant output to track (match) as much as possible the output of the reference model. ROSFC uses a *static* output-error feedback while DDOFC uses a *dynamic* output one. DDOFC presents also an implementation advantage: the reference model does not need to be run in the real-time as is the case for ROSFC. As a consequence, the final proposed control is DDOFC and will be fully presented in what follows. ROSFC is briefly given in Appendix A for comparison purpose. The DDOFC is introduced below.

4.1 | Selection of the reference model

In this subsection, the reference model is designed according to classic robustness rules (see, e.g., [9], [28]). To ensure the *desired performances*, the poles of the open-loop plant $H(s)$ are horizontally shifted to left in the complex plane until getting the desired damping (over 10%) (in Fig. 8). The unstable zeros of the control model are also shifted to the left plane. The other stable zeros are not shifted. The transfer function of the obtained reference model is given in Appendix C. Dynamic responses given in Fig. 8 show the difference between the behaviors of the reference and control models. The controller should be synthesized in order to fill-in this gap.

Let

$$\begin{aligned} \dot{x}_r &= A_r x_r + B_r u_r \\ y_r &= C_r x_r \end{aligned} \tag{6}$$

be one of the minimal state-representations of the reference model.

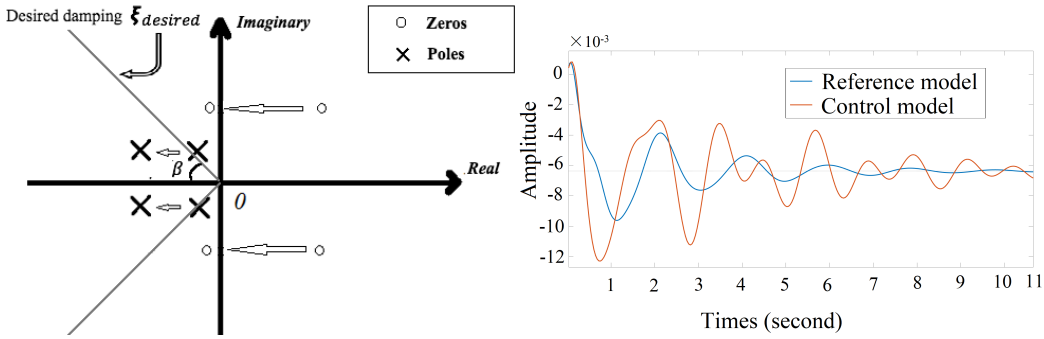

FIGURE 8 Reference model design and step responses

4.2 | DDOFC structure

As shown in Fig. 9, the DDOFC is a dynamic bloc feeded by the measured output of the plant H(s). The red box in that figure corresponds to a state-representation of the regulator

$$\begin{aligned} \dot{x}_c &= A_c x_c + B_c u_c \\ y_c &= C_c x_c \end{aligned} \tag{7}$$

where the matrices A_c, B_c, C_c are thus to be computed.

The above output feedback implementation avoids state estimation. Indeed, for implementation, only the measurement $y = \Delta\theta$ is needed. The resulting closed-loop is the green box in the same figure which does not contain the reference model. As already mentioned, this is an important advantage against alternative ROSFC presented in Appendix A.

From Fig. 9, and (2), (6), (7) , the *augmented* state-space system to be used for controller synthesis is

$$\begin{aligned} \dot{X} &= \bar{A}X + \bar{B}u_r \\ Y &= \bar{C}X, \end{aligned} \tag{8}$$

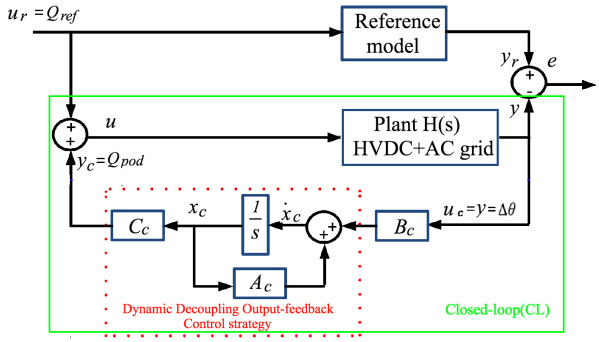

FIGURE 9 The structure of the DDOFC.

where

$$X(t) = \begin{bmatrix} x \\ x_r \\ x_c \end{bmatrix}, \bar{A} = \begin{bmatrix} A & 0 & -BC_c \\ 0 & A_r & 0 \\ B_c C & 0 & A_c \end{bmatrix}, \bar{B} = \begin{bmatrix} B \\ B_r \\ 0 \end{bmatrix}, \bar{C} = \begin{bmatrix} -C \\ C_r \\ 0 \end{bmatrix}^T.$$

4.3 | DDOFC gains computation for stability and robustness

The model-matching problem formulated above is equivalent to a disturbance rejection problem: $||T_{u_r e}||_\infty \le \gamma$. Indeed, if the transfer from u_r to e in Fig. 9 is minimal, the model matching is maximal. The norm minimization problem is commonly used in robust control theory and it is solved here by the following result.

Theorem 1: System (8) is asymptotically stable and γ is minimized if and only if there exist positive definite symmetric matrices $Q, Z \in \Re^{(n+n_r)\times(n+n_r)}$, non singular matrices $\widehat{A}, \widehat{B}, \widehat{C} \in \Re^{(n+n_r)\times(n+n_r)}$ such that the LMIs (9) are satisfied.

$$\begin{bmatrix} \phi_1 + \phi_1^T & \widehat{A}^T + \begin{bmatrix} A & 0 \\ 0 & A_r \end{bmatrix} & \begin{bmatrix} B \\ B_r \end{bmatrix} & Q\begin{bmatrix} -C^T \\ C_r^T \end{bmatrix} \\ * & \phi_2 + \phi_2^T & Z\begin{bmatrix} 0 \\ B_r \end{bmatrix} + \widehat{B} & \begin{bmatrix} -C^T \\ C_r^T \end{bmatrix} \\ * & * & -\gamma I & 0 \\ * & * & 0 & -\gamma I \end{bmatrix} \le 0, \begin{bmatrix} Q & I \\ I & Z \end{bmatrix} \ge 0, \tag{9}$$

where

$$\phi_1 = \begin{bmatrix} A & 0 \\ 0 & A_r \end{bmatrix} Q + \begin{bmatrix} -B\widehat{C} \\ 0 \end{bmatrix}, \phi_2 = Z\begin{bmatrix} A & 0 \\ 0 & A_r \end{bmatrix} + \begin{bmatrix} B\widehat{B}C \\ 0 \end{bmatrix}^T.$$

Once unknown variables $Q, Z, \widehat{A}, \widehat{B}, \widehat{C}$ are computed to satisfy (9), the state matrices of the controller are

$$A_c = N^{-1}\bar{A}M^{-T}, B_c = N^{-1}\widehat{B}, C_c = \widehat{C}M^{-T}, \tag{10}$$

where

$$\bar{A} = \widehat{A} - Z\begin{bmatrix} A & 0 \\ 0 & A_r \end{bmatrix} Q - N\begin{bmatrix} B_c C \\ 0 \end{bmatrix}^T Q - Z\begin{bmatrix} BC_c \\ 0 \end{bmatrix} M^T \text{ and } NM = I - ZQ. \tag{11}$$

Proof. Based on Bounded real lemma [29, 15], the closed-loop system is stable if and only if there exists a symmetric matrix $W \in \Re^{2(n+n_r)\times 2(n+n_r)}$ such that,

$$\begin{bmatrix} \bar{A}^T W + W\bar{A} & W\bar{B} & \bar{C}^T \\ \bar{B}^T W & -\gamma I & 0 \\ \bar{C} & 0 & -\gamma I \end{bmatrix} \le 0, W \ge 0. \tag{12}$$

It can be seen that (12) is a Bilinear Matrix Inequality (BMI). To convert it to LMI, the variables substitution method based on [30] is used. Let the partition of W and W^{-1} be

$$W = \begin{bmatrix} Z & N \\ N^T & \star \end{bmatrix}, W^{-1} = \begin{bmatrix} Q & M \\ M^T & \star \end{bmatrix} \tag{13}$$

where $Q, Z \in \Re^{(n+n_r)\times(n+n_r)}$ are positive definite symmetric matrices, $M, N \in \Re^{(n+n_r)\times(n+n_r)}$ are full matrices and $\star$ are unknown matrices. Let

$$\prod_1 = \begin{bmatrix} Q & I \\ M^T & 0 \end{bmatrix}, \prod_2 = \begin{bmatrix} I & Z \\ 0 & N^T \end{bmatrix} \quad . \tag{14}$$

From $WW^{-1} = I$, it can be inferred $\prod_2 = W\prod_1$.

In this case, $\prod_2^T W\bar{A} = \prod_2^T \bar{A}\prod_1$, so that,

$$\prod_2^T \bar{A}\prod_1 = \begin{bmatrix} I & 0 \\ Z & N \end{bmatrix}\begin{bmatrix} A & 0 & -BC_c \\ 0 & A_r & 0 \\ B_c C & 0 & A_c \end{bmatrix}\begin{bmatrix} Q & I \\ M^T & 0 \end{bmatrix} = \begin{bmatrix} \begin{bmatrix} A & 0 \\ 0 & A_r \end{bmatrix} Q + \begin{bmatrix} -BB_c \\ 0 \end{bmatrix} M^T & \begin{bmatrix} A & 0 \\ 0 & A_r \end{bmatrix} \\ Q_1 & Q_2 \end{bmatrix} \tag{15}$$

and,

$$\prod_1^T W\bar{B} = \prod_2^T \bar{B}\prod_1 = \begin{bmatrix} I & 0 \\ Z & N \end{bmatrix}\begin{bmatrix} B \\ B_r \\ 0 \end{bmatrix} = \begin{bmatrix} B \\ B_r \\ Z\begin{bmatrix} B \\ B_r \end{bmatrix} \end{bmatrix}, \prod_1^T \bar{C} = \left[\begin{bmatrix} -C & C_r & C \end{bmatrix}\begin{bmatrix} Q & I \\ M^T & 0 \end{bmatrix}\right]^T \begin{bmatrix} Q\begin{bmatrix} -C^T \\ C_r^T \end{bmatrix} \\ -C_r^T \\ C_r^T \end{bmatrix} \quad . \tag{16}$$

where,

$$Q_1 = Z\begin{bmatrix} A & 0 \\ 0 & A_r \end{bmatrix} Q + N\begin{bmatrix} B_c & C & 0 \end{bmatrix} Q + Z\begin{bmatrix} -BC_c \\ 0 \end{bmatrix} M^T + NA_cM^T, Q_2 = Z\begin{bmatrix} A & 0 \\ 0 & A_r \end{bmatrix} + N\begin{bmatrix} B_c & C & 0 \end{bmatrix} . \quad (17)$$

Thus,

$$\hat{A} = Z\begin{bmatrix} A & 0 \\ 0 & A_r \end{bmatrix} Q + N\begin{bmatrix} B_c & C & 0 \end{bmatrix} Q + Z\begin{bmatrix} -BC_c \\ 0 \end{bmatrix} M^T + NA_cM^T, \hat{B} = NB_c, \hat{C} = C_cM^T . \quad (18)$$

Therefore, (12) are equivalent to (9) which proves Theorem 1.

4.4 | Uncertainty analysis in case of different operation points

In order to analyze and improve the closed-loop behavior in case of model uncertainties, different operating points are studied in this section. They correspond to different disturbed grid situations which usually happen in realistic power systems:

1. Inverse the HVDC active power flow direction and amount (from $+800MW$ to $-200MW$);
2. 30% increase of the load of the terminal bus of generator GE_911 (the generator with highest participation to the less damped mode 2);
3. Tripping generator GE_914 which is close to generator GE_911;
4. Tripping 4 lines close to the generator GE_911 (transit 213MW, 137MW, -41MW,-118MW on these lines at the moment of the trip).

These cases correspond to the first class of the robustness issue mentioned before (i.e., the parametric case). The behavior of the regulators in all these disturbed grid situations called *robust operation cases* in the sequel will be compared with results of *nominal operation case*. The linearization for each robust operation case at an equilibrium point is done to obtain state-space matrices. *The average rate of change* σ of A, B and C state-space matrices of each robust cases against the nominal case are shown in Fig. 10. Neglectable variations (less than 0.8%) have been noticed for B matrix compared to the ones of A and C matrices.

More precisely, if the nominal case state matrix is $A = [a_{ij}]$, and the robust case state matrix is $\tilde{A_{ij}} = [\tilde{a_{ij}}]$, then the rate of change Δ and the average rate of change σ are defined as in (19).

$$\Delta = \sum_{i=1}\sum_{j=1} \frac{\left|a_{ij} - \tilde{a_{ij}}\right|}{\left|a_{ij}\right|}, \sigma = \frac{\Delta}{i * j}. \quad (19)$$

4.5 | Robustness based on LMI conditions

In order to enhance the robustness of the controller to face different operation points, or, roughly speaking, to ensure the effectiveness of the controller, the uncertainty terms quantified in the previous section are considered here for the control synthesis.

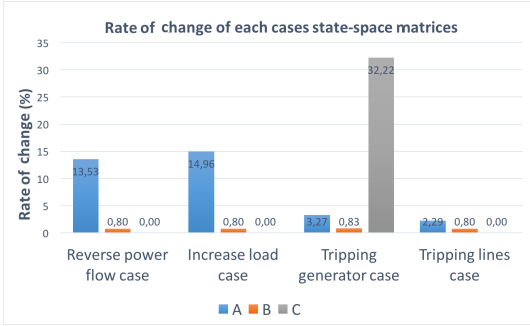

FIGURE 10 Uncertainty analysis: average rate of change of A, B and C.

Then, the linear system affected by uncertainties is

$$\begin{aligned} \dot{x} &= (A + \Delta A)x + Bu \\ y &= (C + \Delta C)x. \end{aligned} \tag{20}$$

Theorem 2: System (20) is asymptotically stabilizable if there exist symmetric and positive definite matrix P, some constant $\zeta > 0$ and scalars ϵ_1 and ϵ_2, such that the following LMI is satisfied,

$$\begin{bmatrix} -2\zeta I & \zeta A_o + P & \zeta I & \zeta M_1 & \zeta BKM_2 \\ * & -P + \delta & 0 & 0 & 0 \\ * & * & -P & 0 & 0 \\ * & * & * & -\epsilon_1 I & 0 \\ * & * & * & * & -\epsilon_2 I \end{bmatrix} \leq 0 \tag{21}$$

In this paper, thresholds $\Delta A \leq 14.96\%$ and $\Delta C \leq 32.22\%$ deduced in previous section are now transformed into the LMI: $F_1^T F_1 \leq I$, where $\Delta A = M_1 F_1 N_1$, $\Delta C = M_2 F_2 N_2$, M_1, M_2, N_1, and N_2 are known real constant matrices which characterize the parameter uncertainties for the nominal matrices A, and C. F_1, and F_2 are unknown real matrices with Lebesgue measurable elements, satisfying $F_1^T F_1 \leq I$.

Proof. The proof can be given directly from [31], [32].

5 | VALIDATION TESTS FOR Q MODULATION

The designed controllers are fully validated on the test system in this section. To easily compare the effectiveness between controllers, first, the controllers are applied on the linearized full model in Matlab. Second, they are tested on the nonlinear benchmark in Eurostag.

5.1 | Linearized full model validation

In this section, controllers are tested in Matlab with linearized full model in the nominal operation case. Step responses of angle difference $\Delta\theta$ with different controllers are compared in Fig. 11. In the zoomed figure on the rectangle region, it can be seen that starting from the $t = 8s$, mode 2 is observable and its frequency can be measured from two peaks. The DDOFC POD and LQG POD provide more damping compared to the other POD controllers. The classic and RSOFC POD provide even the same damping as of the open-loop. In addition, from $t = 2s$ to $t = 4s$, mode 5 can be observed: the DDFOC POD, LQG POD and mixed sensitivity H_∞ POD, which have less undershoot than the others POD controllers provide sufficient damping for this mode. It should be noticed that, from $t = 1s$ to $t = 3s$, mode 1 (with its frequency 1.3Hz) is observable (in the curve with LQG POD) (see zoomed figure in the middle of above one). This oscillation also exists in the open-loop curve. Thus, it can be concluded that the proposed DDOFC POD guarantees a sufficient damping in a wide frequency band.

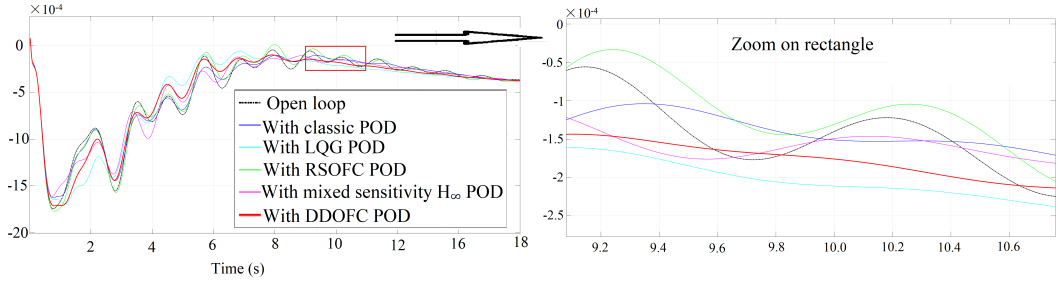

FIGURE 11 Comparison with linearized full model.

The closed-loop modes are shown in Table 5. It can be seen that, the classic POD improves a little the damping of mode 2, but disturbs mode 4. The DDOFC POD, LQG POD and mixed sensitivity H_∞ POD improve the damping of each mode over 10%. To be precise, the LQG POD gives the highest value of damping on mode 3; the mixed sensitivity H_∞ POD provides accepted dampings of mode 4 and 5; RSOFC POD decreases each mode damping except the one of mode 5; the DDOFC POD satisfies the target damping of modes 1 and 2 without disturbing the others. It can also be seen that the proposed DDOFC POD fulfils the damping requirement.

Although calculating dampings of modes after linearizing their closed-loop systems with different controllers at an equilibrium point is an intuitive way to evaluate the effectiveness of each controller, the nonlinear dynamic features cannot be evaluated in this way and should be excited by stronger disturbances as the short-circuits studied in the next section.

5.2 | Nonlinear system validation

In order to test the performances and robustness of new synthesized controllers, the latter are tested on nonlinear model with Eurostag software. Both ***nominal operation case*** and ***robust operation cases*** as explained in Section 4.4 are considered. For all tests, a balanced three-phase ground short-circuit at bus FVLAR1-2 which is the terminal bus of generator GE_918 (see Fig. 2) is considered. Because it is close to generator GE_911 which is the most participating machine in mode 2 (see Table 1), this disturbance excites the modes of interest. In the nonlinear test, much more attention is paid to the generator speed, especially for the most participating machine(s) in the modes of interest.

TABLE 5 Comparison of damping

No.	ξ open-loop (%)	ξ with classic POD (%)	ξ with LQG POD (%)	ξ with Mixed sensitivity H_∞ POD (%)	ξ with RSOFC POD(%)	ξ with DDOFC POD (%)
1	19.5	30.5	21.7	20.3	18.6	23.3
2	4.5	6.1	10.9	11.6	4.2	12.6
3	10.1	12.0	14.9	12.3	9.6	10.8
4	8.3	8.1	11.4	12.4	7.9	10.6
5	10.1	12.4	13.6	14.9	14.2	14.1

5.2.1 | Nominal operation test

A comparison between controllers of the nominal operation case is shown in Fig. 12.

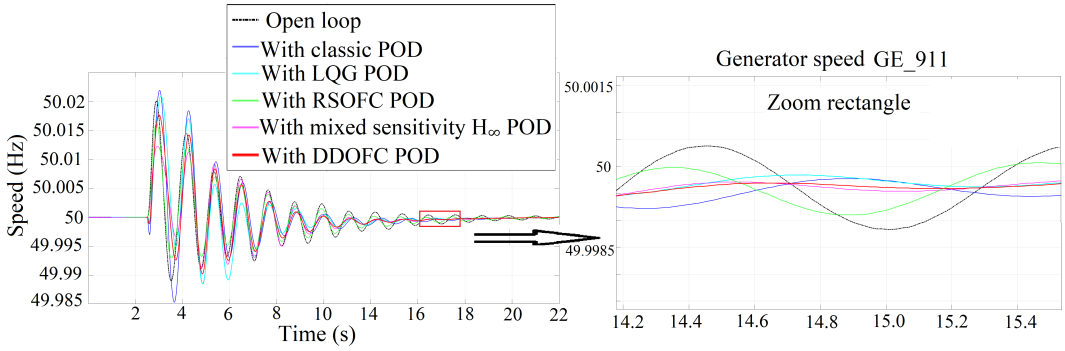

FIGURE 12 Nonlinear nominal operation case.

From the zoomed figure in Fig. 12, it can be seen that for mode 2 (it is recognized by measuring the frequency between peaks in curves from the 8^{th} swing), the DDOFC POD and mixed sensitivity H_∞ provide more damping compared with the other controllers. From $t = 3s$, there are the contributions of several modes mixed with nonlinear dynamics. It can be seen that the DDOFC, mixed sensitivity H_∞, and LQG POD provide more damping than RSOFC and classic POD. However, from the 4^{th} to the 8^{th} swing (the period in which mode 1 can be observed), the damping provided by mixed sensitivity H_∞ POD is less than by DDOFC POD. These behaviours confirm the modal analysis estimation in Table 5.

In addition, the proposed controllers must have the ability to deal with different operation points of the system to settle a good trade-off between performance and robustness. This is checked by the robustness tests reported in the next section.

5.2.2 | Robustness tests

In order to investigate the behaviors in the case of system uncertainties, different disturbed grid situations defined in Section 4.4) are now used. The same short-circuit used in the nominal operation case at the terminal bus FVLAR1-2 is considered to excite the dynamics.

Responses obtained with the same controllers considered above are now shown in Fig. 13, 14, 15, 16 for the following situations:

- **Inverse power flow case:** In Fig. 13, the performance of RSOFC POD and mixed sensitivity H_∞ POD are almost the same with DDOFC POD from $t = 12s$ (mode 2). It can be seen that it provides more damping than the other controllers. From the 3^{rd} swing, mode 4 is dominant. For this mode, although the RSOFC POD controller dampes more than the other controllers, its damping in the nominal operation case is insufficient. Notice that from $t = 3s$ to $t = 5s$, although the amplitude of oscillation with mixed sensitivity H_∞ POD is smaller than the one with DDOFC POD, its curve has one more tiny swing at $t = 3.5s$ (see zoomed figure in the middle). This means that the mixed sensitivity H_∞ POD may excite other nonlinear dynamics in the system. This phenomenon also appears in following increasing load case. The oscillation with classic POD, in this case, is even higher than in open-loop. Besides, the damping of the other modes is also decreased. This test shows that the proposed DDOFC POD have the ability to handle the uncertainties in reverse power flow situation without losing damping/performance for all modes.

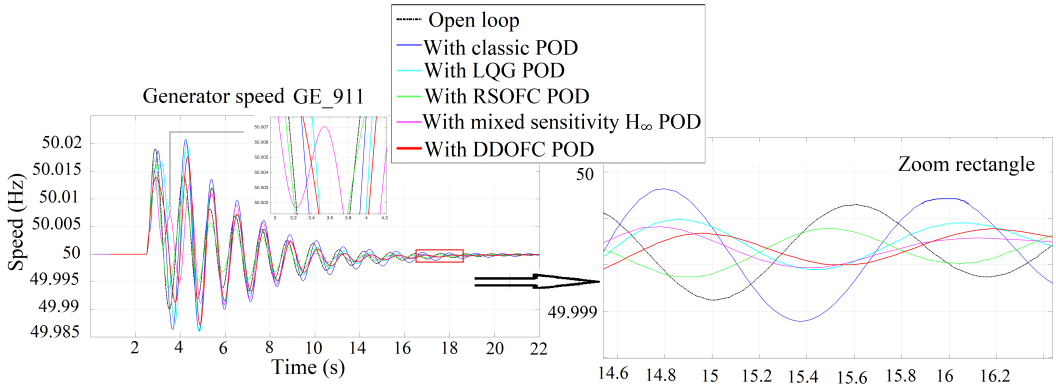

FIGURE 13 Reverse power flow case.

- **Increased load case:** In Fig. 14, from $t = 12s$ (mode 2), the mixed sensitivity H_∞, the LQG POD and the DDOFC POD provide the same accepted damping compared with the other controllers. However, in the middle of the curves (from the 3^{rd} to the 5^{th} swing), the damping provided by mixed sensitivity H_∞ POD is not enough for mode 4. Besides, the overshoot of the curve with LQG POD in the first swing is not desirable. Although that the RSOFC POD provides less damping than the classic POD, its nonlinear dynamics in first two swings is acceptable. According to this test, in increasing load situation, the DDOFC POD is still the only controller to satisfy all requirements.
- **Tripping generator case:** In Fig. 15, from the zoomed picture, it can be seen that, during the first two swings, the LQG POD along with classic POD even increases the oscillations compared to open-loop. They lack of robustness to face these nonlinearities. The DDOFC, mixed sensitivity H_∞ and LQG POD, from $t = 12s$ (mode 2), have damping advantages against the other controllers. In addition, from the 3^{th} to the 6^{th} swing where mode 1 is dominant, DDOFC POD provides more damping than mixed sensitivity H_∞, RSOFC POD, and LQG POD. For the tripping

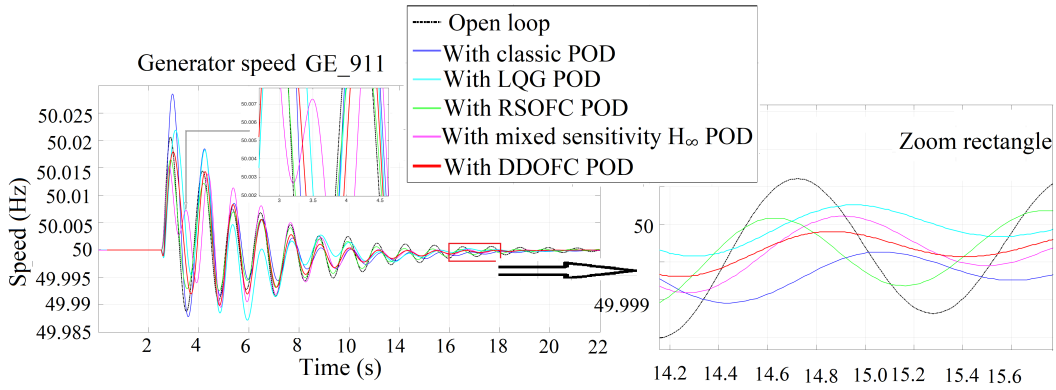

FIGURE 14 Increase load case.

generator case, the best results are ensured by DDOFC POD.

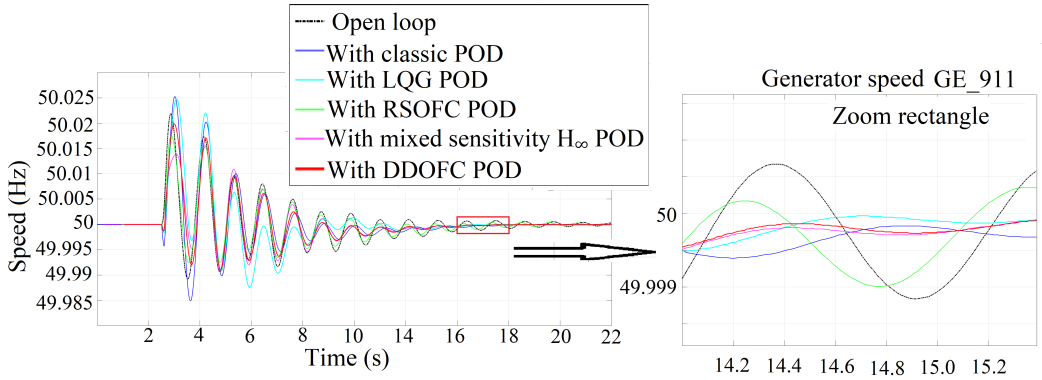

FIGURE 15 Tripping generator case.

- **Tripping lines case:** In Fig. 16, in first two swings of nonlinear dynamic response, despite the fact that the mixed sensitivity H_∞ POD response is the most damped one, the damping for mode 1 (from the 4^{th} to the 8^{th} swing) is less than the one obtained with the classic POD, the LQG POD, and the DDOFC POD. Besides, in the zoomed figure, mode 2 can be observed and it is more damped with DDOFC than with mixed sensitivity H_∞ POD and RSOFC POD. Moreover, for mode 2, although LQG POD seems to provide sufficient damping, the oscillation in the first two swings is even higher than open-loop. Thus, the DDOFC POD is again the controller which provides the best results in this case also.

Thus, among all these tests, the proposed DDOFC POD controller has the robustness to deal with different operation points which also provides sufficient damping for each case. This control strategy is selected as best solution and will be next applied to coordinate active and reactive power modulation as final control solution.

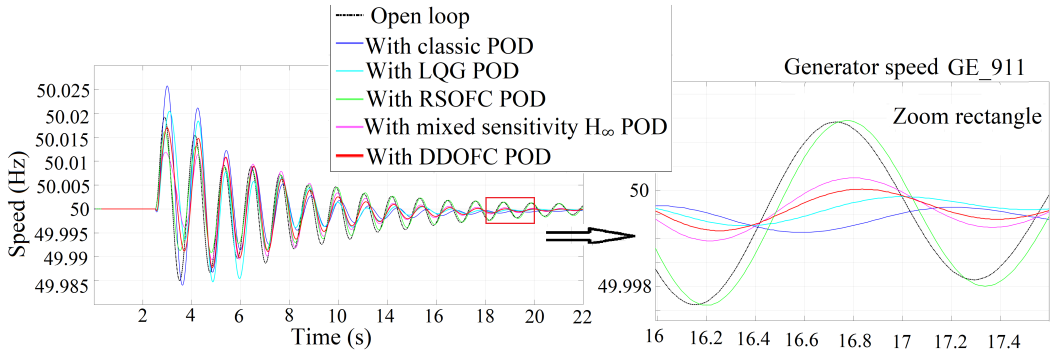

FIGURE 16 Tripping lines case.

6 | COORDINATED P/Q MODULATION

As the VSC-HVDC link controls in an independent manner the transmitted active and reactive powers, in order to fully take advantage of power modulations to improve oscillations damping and robustness, the coordination of reactive Q and active P power modulation is achieved in this section. The same input signal as for the reactive power modulation controller is used in this coordinated controller. The proposed control approach DDOFC is applied to modulate both the active and reactive powers in this section. As the coordinated controller has one input and two outputs, a Single-Input Multi-Output (SIMO) modulation POD controller is synthesized in what follows. That is, the input signal of this SIMO controller is the same with only Q modulation POD controller ($\Delta\theta$). The output of the POD controller is reactive power and also active power modulation signals as shown in Fig. 17.

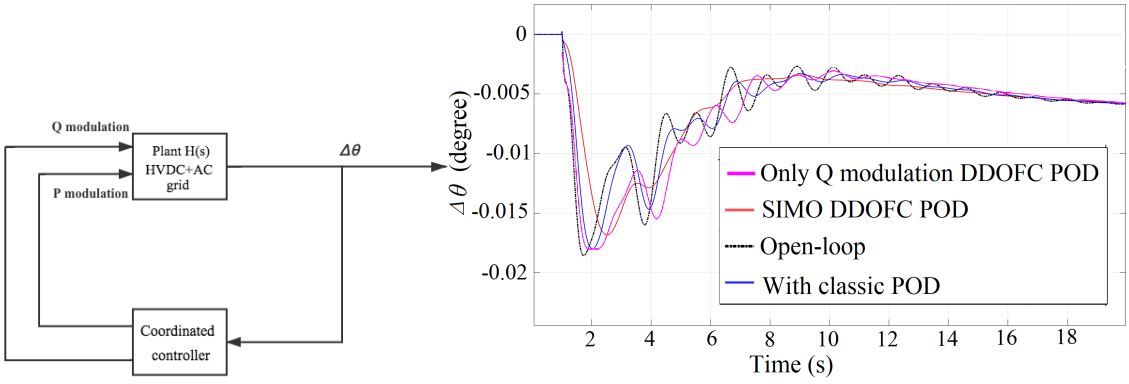

FIGURE 17 Structure of the SIMO coordinated modulation POD and Comparison of SIMO modulation PODs in linearized model.

The same Bode plot fitting methodology mentioned in Section 2.2 is adopted to obtain a reduced-order control model. The controller design process is similar to the one explained before for Q modulation.

7 | VALIDATION TESTS FOR COORDINATED P/Q POD CONTROLLER

The classic P/Q coordinated POD controller is designed to compare its effectiveness with the proposed SIMO modulation POD. Its principle for parameters tuning is the same as the one used for Q modulation.

7.1 | Linearized model validation

The linearized full model validation results are directly presented in this section.

The step response results in Matlab of the closed-loop system of the linearized model with SIMO modulation POD controllers are shown in Fig. 17.

First, notice that classic SIMO modulation POD is more effective than only Q POD modulation. Next, the DDOFC SIMO POD provides better damping than SIMO classic POD. Indeed, from $t = 10s$, oscillation is fully damped, which is not the case with the classic POD.

7.2 | Nonlinear model validation

The proposed SIMO modulation POD controller is also validated in nonlinear simulation with Eurostag in this section. Notice that for this validation, the same short-circuit disturbance (same value and same location) used in Section 5.2.2 is considered. The tests are also divided into two parts: nominal operation case and robust operation cases. The reverse power flow scenarios of Section 5.2.2 is adopted here to test robustness. Results are shown in Fig. 18.

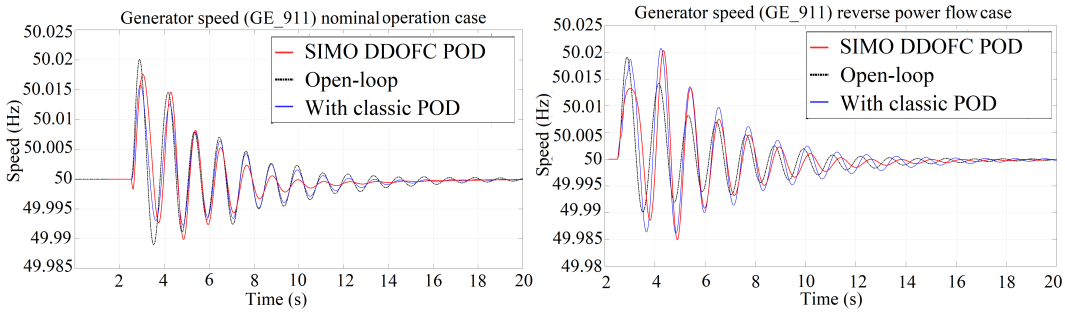

FIGURE 18 Nominal operation case and reverse power flow case with SIMO modulation PODs.

The DDOFC SIMO modulation POD damp less the first 3 nonlinear swings than the classic one. However, it provides better damping of the modes (can be seen from the 4^{th} swing). The classic SIMO modulation POD amplifies the oscillations compared with the open-loop system from the 2^{nd} to the 5^{th} swing (mode 1). However, the damping of target mode 2 is improved (starting from the 7^{th} swing).

From these results, one can conclude that the new DDOFC SIMO modulation POD can significantly improve the damping of target modes-especially mode 2-at more than 15% and much more than the classic POD (less than 8% for mode 2). Although the nonlinear dynamic responses in first several swings of DDOFC SIMO modulation POD controller are less damped than with only Q modulation DDOFC POD (according tests in Section 5.2.2), the damping of mode 1 in these swings is still acceptable (around 10%). Moreover, dampings of modes 2 and 4 are improved compared with Q

modulation and this damping level is maintained in different operation points cases. This is confirmed by validation run for all grid disturbed situations defined in Section 4.3 and presented in Section 5.2.2 which are skipped here because of the lack of the place.

8 | CONCLUSION

A new control method was provided to coordinate active and reactive power modulation of a HVDC link in the particular case where the latter is inserted into an AC meshed grid. In this situation, oscillations are at higher frequencies and unstable zeros were systematically put into evidence. This results in interactions with higher order and nonlinear dynamics. Addressing the usual damping specifications in this new context was a new and hard problem. It was solved here by proposing a new mixed robust model-matching control framework based on LMIs. More specifically, the control was improved at the following levels:

- At the modeling level: a *control model* was used to capture all dynamics of interest in the frequency band of the inter-area modes to be damped. Next, a *reference model* was built to gather *all* control specifications, including cancellation of the effect of unstable zeros.
- At the synthesis level: a model-matching robust feedback was proposed to track the reference model in presence of usual grid variations (line/generator trips, modification of operation point, etc) and disturbances (short-circuits).
- At the implementation level: the control was provided into the form of an output feedback in order to use only local measurement of the angles at the HVDC connection points. The state-space realization of the controller can be easily implemented in practice.

This new control framework allowed not only to obtain better results than with the classic POD tuning, but provides also a direct way to establish the trade-off between performances (damping of the inter-area modes of interest) and robustness level (tolerate variations of the grid situations and operating points and disturbance rejection). This fact it is well-known in control theory but was less exploited till now in difficult power systems applications, like the one treated here which requires high level of robustness. The latter is achieved by well chosen poles and zeros shifts, in the synthesis of both reference model and regulator.

Extensive validations were carried out on realistic 19 machines grid situations with a grid professional software (Eurostag). The results prove that the proposed controller has the ability to deal with the target specifications.

Future work will concern hardware-in-the-loop validations.

APPENDIX A: MODEL-MATCHING ROBUST H_∞ STATIC OUTPUT-ERROR FEEDBACK CONTROL (RSOFC)

The resulting structure of the RSOFC is given in Fig. H1.

RSOFC is a static output-error feedback: $u_c = Ke$, where K is the matrix controller gains. It is computed as in the case of DDOFC, by solving a well-chosen set of LMIs.

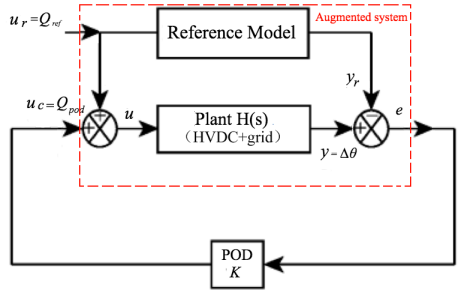

FIGURE H1 The structure of RSOFC.

APPENDIX B: CONTROL MODEL (PLANT H(S))

The transfer function of the control model in Section 2.2 is (22). $n = 12$. Coefficients are given in Table 6.

$$f(s) = \frac{Nco_{n-1}s^{n-1} + \ldots + Nco_1 s + Nco_0}{Dco_n s^n + \ldots + Dco_1 s + Dco_0} \tag{22}$$

TABLE 6 Transfer function of the control model H(s)

i=	12	11	10	9	8	7	6	5	4
Nco	/	0.01504	0.08873	0.6758	- 0.8807	- 88.8	- 763.7	- 6857	- 3.609e04
Dco	1	11.14	240.2	1804	2.02e04	1.071e05	7.974e05	2.945e06	1.582e07

3	2	1	0
- 1.61e05	- 6.049e05	- 1.246e06	- 3.278e06
3.755e07	1.492e08	1.758e08	5.147e08

APPENDIX C: REFERENCE MODEL

The transfer function of the reference model is also in the form (22). $n = 12$. Coefficients are given in Table 7.

ACKNOWLEDGEMENTS

The authors would like to thank China Scholarship Council (CSC) for the financial support to Yankai Xing.

REFERENCES

[1] Analysis of inter-area oscillations of 1*st* december 2016. ENTSO-E SG SPD Report, 2017. https://eepublicdownloads.entsoe.eu/clean-documents/SOC%20documents/Regional_Groups_Continental_Europe/2017/CE_inter-area_

TABLE 7 Transfer function of the reference model

i=	12	11	10	9	8	7	6	5	4
Nr	/	0.02143	0.1264	0.9629	-1.255	-126.5	-1088	-9771	- 5.143e04
Dr	1	19.54	355.5	3773	3.638e04	2.492e05	1.565e06	7.205e06	3.094e07

3	2	1	0
- 2.294e05	- 8.618e05	- 1.776e06	- 4.671e06
9.178e07	2.646e08	4.098e08	7.333e08

oscillations_Dec_1st_2016_PUBLIC_V7.pdf

[2] Latorre H. F., Ghandhari M., and Söder L. Active and reactive power control of a VSC-HVdc [J]. Electric Power Systems Research, 78(10): 1756-1763, 2008.

[3] Arioua L., and Marinescu B. Robust grid oriented control of high voltage DC links embedded in an AC transmission system [J]. International Journal of Robust and Nonlinear Control, 26(9): 1944-1961, 2016.

[4] Arioua L., and Marinescu B. Multivariable control with grid objectives of an HVDC link embedded in a large-scale AC grid [J]. International Journal of Electrical Power and Energy Systems, 72: 99-108, 2015.

[5] IEEE recommended practice for excitation system models for power system stability studies, in IEEE Std 421.5-2016, doi: 10.1109/IEEESTD.2016.7553421, pp.1-207, 2016.

[6] Hoagg J. B., and Bernstein D. S. Nonminimum-phase zeros-much to do about nothing-classical control-revisited part II [J]. IEEE Control Systems Magazine, 27(3): 45-57, 2007.

[7] Xing Y., Aghababa M. P., Marinescu B., and Xavier F. Analysis and control of non-minimum phase behavior in nonlinear AC grids equipped with HVDC Links [C]. In 2019 IEEE PES Innovative Smart Grid Technologies Europe (ISGT-Europe) (pp. 1-5). IEEE, 2019.

[8] J. Renedo, A. Garcia-Cerrada, L. Rouco and L. Sigrist, "Coordinated Design of Supplementary Controllers in VSC-HVDC Multi-Terminal Systems to Damp Electromechanical Oscillations [J]," in IEEE Transactions on Power Systems, vol. 36, no. 1, pp. 712-721, Jan. 2021, doi: 10.1109/TPWRS.2020.3003281.

[9] Skogestad S., and Postlethwaite I. Multivariable feedback control: analysis and design [M]. New York: Wiley, 2007.

[10] Safonov, Michael G., and Chiang, R. Y. A schur method for balanced-truncation model reduction [J]. IEEE Transactions on Automatic Control, vol. 34, no 7, p. 729-733, 1989.

[11] Marinescu B., and Petesch D. Three-level coordination in power system stabilization [J]. Electric Power Systems Research, 111, 40-51, 2014.

[12] Zhou K., Doyle J. C., and Glover K. Robust and optimal control [M]. New Jersey: Prentice-Hall, 1995.

[13] Kanev, S., Scherer, C., Verhaegen, M., and De Schutter, B. Robust output-feedback controller design via local BMI optimization [J]. Automatica, 40(7), 1115-1127, 2004.

[14] Kose I. E., and Jabbari, F. Robust control of linear systems with real parametric uncertainty [J]. Automatica, 35(4), 679-687, 1999.

[15] Boyd S., El Ghaoui L., Feron E., and Balakrishnan V. Linear matrix inequalities in system and control theory. Society for Industrial and Applied Mathematics, 1994.

[16] Dullerud G. E., and Paganini F. A course in robust control theory: a convex approach (Vol. 36). Springer Science and Business Media, 2013.

[17] M. A. Elizondo et al., "Interarea Oscillation Damping Control Using High-Voltage DC Transmission: A Survey [J]," in IEEE Transactions on Power Systems, vol. 33, no. 6, pp. 6915-6923, Nov. 2018, doi: 10.1109/TPWRS.2018.2832227.

[18] R. Preece, J. V. Milanović, A. M. Almutairi and O. Marjanovic, "Damping of inter-area oscillations in mixed AC/DC networks using WAMS based supplementary controller," in IEEE Transactions on Power Systems, vol. 28, no. 2, pp. 1160-1169, May 2013, doi: 10.1109/TPWRS.2012.2207745

[19] S. Azad, R. Iravani, and J. Tate, "Damping inter-area oscillations based on a model predictive control (MPC) HVDC supplementary controller [J]," IEEE Trans. Power Syst., vol. 28, no. 3, pp. 3174—3183, Aug. 2013.

[20] K. Ichikawa, Control System Design Based on Exact Model Matching Techniques [B], Lecture Notes in Control and Information Sciences, Vol. 74, ISBN: 9783540157724, Springer 1985.

[21] Meyer B., and Stubbe M. Eurostag, a single tool for power system simulation [J]. Transmission and Distribution International, 47-52, 1992.

[22] Xing Y., Marinescu B., and Xavier F. Robust research of power oscillations damping controller for HVDC inserted in meshed AC grids [C], 2019 IEEE Milan PowerTech, pp. 1-6, 2019.

[23] Belhocine M., Marinescu B., and Xavier F. Input signal and model structure analysis for the HVDC link POD control [C], 2017 IEEE Manchester PowerTech, pp. 1-6, 2017.

[24] Hassouneh M. A., Lee H. C., and Abed E. H. Washout filters in feedback control: benefits, limitations and extensions [C]. Proceedings of the 2004 American Control Conference. IEEE, 5: 3950-3955, 2004.

[25] Rouco L. Coordinated design of multiple controllers for damping power system oscillations [J]. International Journal of Electrical Power and Energy Systems, 23(7): 517-530, 2001.

[26] Kamwa I., Grondin R., and Trudel G. IEEE PSS2B versus PSS4B: the limits of performance of modern power system stabilizers [J]. IEEE Transactions on Power Systems, 20(2), 903-915, 2005.

[27] Xing Y., Marinescu B., Belhocine M., and Xavier F. Power oscillations damping controller for HVDC inserted in meshed AC grids [C]. 2018 IEEE PES Innovative Smart Grid Technologies Conference Europe (ISGT-Europe), pp.1-6, 2018.

[28] Zhou K., and Doyle J. C. Essentials of robust control [M]. Upper Saddle River, NJ: Prentice hall, 1998.

[29] Duan G-R., and Hai-Hua Y. LMIs in control systems: analysis, design and applications [M]. CRC press, 2013.

[30] Scherer C., Gahinet P., and Chilali M. Multiobjective output-feedback control via LMI optimization [J], IEEE Transactions on Automatic Control, vol. 42, no. 7, pp. 896-911, 1997.

[31] Chen W. H., Yang W., and Lu X. Impulsive observer-based stabilisation of uncertain linear systems [J], IET Control Theory and Applications, vol. 8, no. 3, pp. 149-159, 2014.

[32] Song J. and He S. Robust finite-time H_∞ control for one-sided Lipschitz nonlinear systems via state feedback and output feedback [J], Journal of the Franklin Institute, vol. 352, no. 8, pp. 3250-3266, 2015.